J Mater Sci: Mater Med (2010) 21:1427–1434
DOI 10.1007/s10856-010-4005-9

Nano iron oxide–hydroxyapatite composite ceramics with enhanced radiopacity

M. Ajeesh · B. F. Francis · John Annie · P. R. Harikrishna Varma

Received: 16 November 2009 / Accepted: 18 January 2010 / Published online: 27 February 2010

Abstract Hydroxyapatite has been widely used for a variety of bone filling and augmentation applications. But the poorly resolved X-ray image of certain hydroxyapatite (HA) based implants such as porous blocks and self setting HA cements is a radiological problem to surgeons for monitoring of the implant and early diagnosis complications. In the present work the practical difficulty related to the reduced X-ray opacity was overcome by exploiting the contrast enhancement property of iron oxide nano particles. Sintered nano iron oxide–HA composite ceramics were prepared from powders produced through a co-precipitation route. The phase purity and bioactivity of the composites were analyzed as a function of percentage iron oxide in the composite. The X-ray attenuation of dense and porous composites was compared with pure HA using a C-arm X-ray imaging system and micro computed tomography. In all the prepared composites, HA retains its phase identity and high X-ray opacity as obtained for a composition containing 40 wt% iron oxide. The increased cell viability and cell adhesion nature depicted by the prepared composite offers considerable interest for the material in bone tissue engineering applications.

1 Introduction

Calcium hydroxyapatite{Ca_{10} $(PO4)_6(OH)_2$} is one of the most popular among synthetic calcium phosphate ceramics which have been identified as potential hard tissue implants because of their close structural and chemical resemblance to natural bone mineral phase [1, 2]. Due to the better osteoconductivity, synthetic hydroxyapatite (HA) is considered to be an ideal material as a bone substitute. Porous hydroxyapatite granules and blocks are the most clinically useful forms and are being applied for filling or augmenting a variety of defects in dental and orthopedic field [3]. Though structural and mechanical properties of HA promote its application as a bone filling agent, the incompetently resolved X-ray image of the poorly dense HA material poses a practical problem with respect to immediate and short term post operative monitoring of bone formation by the clinicians. Hence, organic contrast agents like organo bismuth compounds [4] and organo iodine compounds [5] were added to calcium phosphate bone fillers in order to confer radiopacity and thus aid in the radiographic assessment of the implants in vivo. But the problems such as chemo toxicity and incompatibility of organic–inorganic phases can be avoided by the use of inorganic contrast agents. Barium sulphate ($BaSO_4$) and zirconium dioxide (ZrO_2) are two major inorganic radio-opacifying agents [6] used in calcium phosphate bone cements. But these conventional radio-opacifying agents have been shown to evoke a significant pathological response both in vitro and in vivo compared to the one without any of these agents [7, 8]. $BaSO_4$ and ZrO_2 injected intradermally into experimental animals are known to cause foreign body inflammatory reaction [9] and with the release of inflammatory mediators in response [10]. Hence there is a significant interest in developing a new contrast agent having X-ray attenuation capacity to enhance the opacity property of HA without introducing any secondary changes. Recently, iron oxide nano particles have emerged as a potential candidate material for a variety

M. Ajeesh · B. F. Francis · J. Annie · P. R. Harikrishna Varma (✉)
Bioceramics Laboratory, Biomedical Technology Wing, Sree Chitra Tirunal Institute of Medical Sciences and Technology, Thiruvananthapuram, Kerala, India
e-mail: varma@sctimst.ac.in

of medical applications [11, 12, 13, 14]. In order to increase the X-ray opacity of HA, an attempt has been made to utilize these iron oxide nano particles for the fabrication of a phase pure HA–iron oxide composite with better radiopacity than pure HA. Cellular compatibility of the material is an important factor since the novel composite will be of use in providing enhanced radio-contrast at sites of hard tissue reconstruction. So the materials have been evaluated for in vitro toxicity and also for the capability to support adhesion & proliferation of cells.

2 Materials and methods

2.1 Materials

For the synthesis of the material, $FeCl_2{\cdot}4H_2O$ (Merck, Germany), $FeCl_3$ (Merck, Germany), $Ca(NO_3)_2{\cdot}4H_2O$ (Rankem, India), $(NH_4)H_2PO_4$ (Rankem, India) and 25% aqueous NH_4OH (SD Fine Chemicals, India) and 35% HCl (SD Fine Chemicals, India) had been used. 3-(4,5-Dimethyl thiazol-2-yl)-2,5 diphenyltetrazolium bromide (Sigma-Aldrich, USA), and streptomycin (Invitrogen, USA) Fetal bovine serum (Invitrogen, USA) were used for the MTT assay and cell adhesion studies.

2.2 Composite preparation

The synthesis of iron oxide nano particles along with HA was carried out by co-precipitating iron salt and calcium phosphate precursors in alkaline medium. The iron salt solution was freshly prepared in an acidic medium of HCl using $FeCl_2{\cdot}4H_2O$ and $FeCl_3$ in the ratio of 1:2. The $Ca(NO_3)_2{\cdot}4H_2O$ and $(NH_4)H_2PO_4$ solutions were taken in such a way as to get the Ca/P ratio of 1.67.

The Ca $(NO_3)_2{\cdot}4H_2O$ solution was mixed with iron salt solution at constant stirring until the required temperature 70°C was reached. The pH of the above solution was then slowly increased to 11 by adding 25% ammonia solution together with $(NH_4)H_2PO_4$. The addition was completed in 3 h at constant stirring under N_2 atmosphere. After the complete addition, temperature was increased to 80°C to eliminate the excess ammonia. The system was aged for 24 h at room temperature, after which the precipitate was washed three times with distilled water and centrifuged. The centrifuged particles were redispersed in ethanol medium and magnetically separated.

The separated HA with magnetic nanoparticles were further diluted with ethanol and ultrasonicated for 30 min followed by centrifugation and vacuum drying at 50°C. HA with 20 and 40 wt% of crystallized iron oxide were thus synthesized as a function of chemical composition (designated as HA20Fe and HA40Fe). The as-prepared samples were filled in a silicon tube and compacted in a cold isostatic press (EPSI, Belgium) so as to get a cylindrical shape having 3 cm height and 5 mm radius. Later the cylindrical pellets were cut using a low speed saw and sintered at 1200°C for 2 h in normal air atmosphere to get dense HA–iron oxide ceramic–ceramic composite discs.

2.3 Characterization of prepared composite

The phase analysis of both HA20Fe and HA40Fe were done at room temperature and at high temperature (1200°C). The crystal structure was determined by analyzing the position and intensities of diffraction peak typically observed in the range of diffraction angle $2\theta = 20–70°$. The samples were scanned between 20 and 70 at a rate of $5°\ min^{-1}$ with a step wise of 0.1° using Cu Kα1 radiation at 40 kV and a 30 mA current strength (Siemens D-5005, Germany). The method is also used for evaluating the particle size by analyzing the width and shape of the peak profile.

To know the fate of nano iron oxide particles in the as prepared as well as in the sintered state, HA40Fe was taken as the representative of the prepared composites and viewed under TEM (HRTEM FEI Technai G2 20 S-TWIN, USA). The magnetically separated and thoroughly washed as prepared samples were dispersed in deionized water followed by ultrasonication for 5 min. A very small amount of sample dispersed in deionized water was allowed to slowly dry on a formvar-coated copper grid for TEM observation. Sintered composite was processed for TEM analysis (LIBRA 200MC Carl Ziess, UK) after several thinning procedures including dimpling and ion milling (Gatan instruments, India).

The morphology of the as prepared HA40Fe composite particles was analyzed using an FEG-ESEM (XL 30 ESEM FEG, Philips, Netherlands). HA40Fe after sintering at 1200°C was gold coated in an ion sputter (E101, Hitachi, Japan) and observed through scanning electron microscope (FEI Quanta 200, Netherlands) attached with X-ray micro analysis. The distribution of both phase as well as the chemical identity was analyzed from the backscattered image and EDS spectra obtained.

2.4 Biomineralisation—in vitro

The bioactive behavior of the composite, the apatite growth on the surface was primarily assessed through a biomimetic approach. The as prepared HA40Fe pellets, sintered pellets of HA20Fe and HA40Fe were immersed in 1.5 ml simulated body fluid (SBF), a metastable solution having inorganic ion concentration similar to those of human extra cellular fluid [15]. The pellets were retrieved after 4 days immersion, washed in deionised water, gold coated and the calcium phosphate growth over the surface was analyzed

by scanning electron microscope (FEI quanta 200 Netherlands) with X ray microanalysis.

2.5 Cytotoxicity

Cytotoxicity/cell viability of the composite in the as prepared as well as sintered samples was analyzed by MTT assay using human osteosarcoma cell line (HOS). Metabolic activity of the cells were measured by measuring the ability of cells to reduce 3-(4,5-Dimethyl thiazol-2-yl)-2,5 diphenyltetrazolium bromide (MTT) to purple colored Formosan crystals. Material extract was prepared by incubating 0.1 g/ml of four samples namely pure HA, as prepared HA40Fe, sintered HA 20Fe and HA40Fe with culture medium containing 10% FBS at 37°C for 24–26 h. Material extracts were added to sub-confluent HOS monolayer in a 96 well culture plate and incubated at 37°C for 24 h and was replaced with 200 µl fresh culture medium containing 500 µl MTT (10 mg/ml in serum free medium). After 4 h the medium having MTT was discarded and 200 µl of isopropanol was added and kept for 20 min to lyses the cells. The color developed was quantified by measuring the absorbance at 570 nm using micro plate reader. (Biotech, Power wave XS, USA). All experiments were done in triplicate and the statistical analysis was done by using a two tailed paired *t*-test with a level of 95% accuracy.

2.6 Cell adhesion

Cell adhesion was performed using New Zealand White Rabbit adipose tissue-derived Mesenchyme stem cells (ADMSCs). From subcutaneous fat tissue, ADMSCs were isolated by 0.2% Collagenase Type I (Invitrogen,USA) digestion and seeded on sintered composite discs of HA20Fe and HA40Fe, placed in 6-well Tissue Culture plate and maintained with α-MEM containing 10% Fetal Bovine Serum and 50 units/ml of penicillin and 50 µg/ml of streptomycin at 37°C under 5% CO_2 atmosphere. The cell-seeded ceramic composite samples were evaluated over a period of 3 and 7 days using ESEM (FEI quanta 200 Netherlands) to assess cell morphology & adhesion.

2.7 X ray attenuation

The efficacy of sintered dense samples to attenuate radiation and create contrast in X-ray film was compared with pure hydroxyapatite. Pure HA, the composite with 20, 40 and 60 wt% iron oxide having 2 mm thickness and 4.8 mm radius were placed in a polythene sheet together with an aluminum wedge with five thickness steps between 1 and 5 mm. The samples were imaged in air at a distance of 0.9 m from the X-ray tube focus with voltage 70 kV and 63 mA. Photoshop™ (Adobe Inc software, US) were used to measure the gray scale of the specimens, averaged over an area 5 × 5 pixel.

The X-ray opacity of the sintered porous samples were further confirmed by examining the 2D slices of the composite with an X-ray microtomograph (µCT 40 Scanco Medial AG, Switzerland) The porous blocks of HA, HA20Fe and HA40Fe samples were generated by mixing the powdered samples with a pore former followed by uniaxial compaction and sintering. The three blocks were scanned together after stacking the samples in a 2 cm micro CT sample holder so as to compare the contrast enhancement in a single pass of X-ray beam.

3 Results

3.1 Phase analysis

Figure 1 shows the X-ray diffraction pattern of as prepared HA20Fe and HA40Fe. The (311), (220), (511), (440) peaks correspond to cubic inverse spinel structure of magnetite phase of (Fe_3O_4) and the (211), (112), (300), (002) peaks belong to the hexagonal HA structure. The particle size of magnetite analyzed by Williamsons–Hall method [16] was found to be around 20 nm. The XRD pattern of the sintered HA20Fe and HA40Fe are shown in Fig. 2. The peak analysis indicates the presence of well crystalline rhombohedral hematite (Fe_2O_3) phase of iron oxide and hexagonal HA crystal structures with no tertiary phase. The XRD pattern analysis explains the existence of magnetite (Fe_3O_4) phase of iron oxide in the as prepared sample and hematite (α-Fe_2O_3) phase in the sintered state. The increase in relative peak intensities with respect to the increased percentage of composition of hematite suggests that the

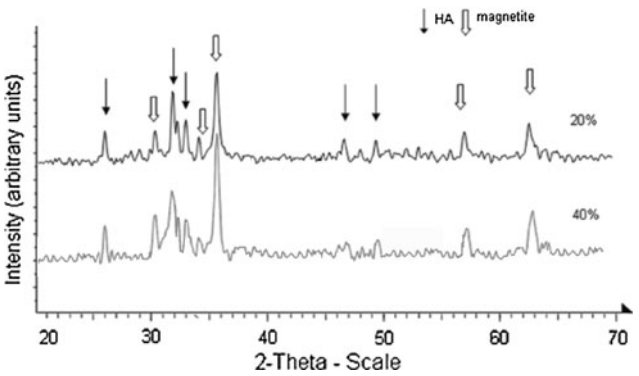

Fig. 1 X-ray diffraction pattern of as prepared composite showing characteristic peaks for HA [Ca_5 $(PO_4)_3OH$] and magnetite (Fe_3O_4) and matching to that of PDF 09-432 and 19-629

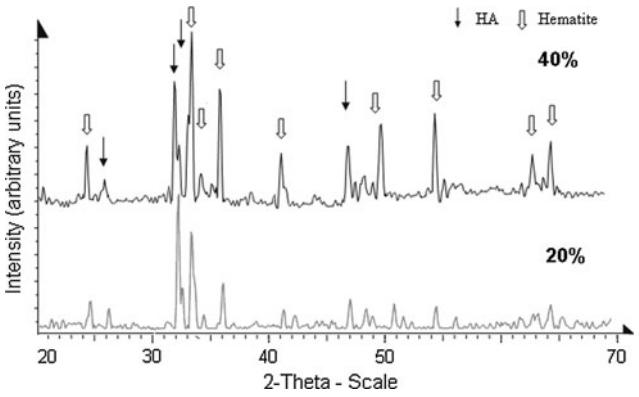

Fig. 2 X-ray diffraction pattern of composites sintered at 1200°C exhibit crystalline pattern of HA [Ca_5 $(PO_4)_3OH$] and hematite (Fe_2O_3) (PDF file no 09-432 and 33-664, respectively)

formation of iron oxide takes place together with HA without affecting the phase purity of the later.

3.2 Transmission electron microscopy

The TEM micrograph of the as prepared HA40Fe particles is as shown in Fig. 3a. The micrograph showed the dispersion of iron oxide nano particles in 100 × 50 nm HA beads. The more focused image in the inset unveil the distribution of black nano iron oxide particles having size less than 20 nm in the grayish HA matrix. The TEM image of the thin section of sintered HA40Fe (Fig. 3b) elucidate the dispersion of dark spherical iron oxide particles in loosely sintered grayish HA grains. At 1200, the particle agglomeration during the process of sintering brings about a particle size of 150 nm compared to the as prepared particles (∼20 nm particle size).

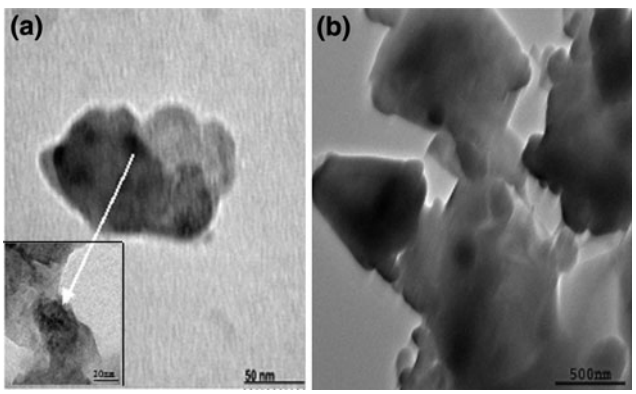

Fig. 3 TEM images of **a** the as prepared composite. High magnification image in inset shows the distribution of nano iron oxide particles (*black in colour*) in white HA matrix. **b** The sintered sample after dimpling and iron milling

3.3 Scanning electron microscopy

Figure 4b shows the SEM image of the as precipitated HA40Fe at high magnification using the ESEM-FEG. The typical acicular morphology of HA is clear in the high magnification image, but the iron oxide particles are not distinctively clear which may be due to its still smaller size. The back scattered SEM images of same sample after sintering is as shown in Fig. 4a. The white sintered grains of hematite (α-Fe_2O_3), grey hydroxyapatite grains with distinct grain boundaries are clear in the observed images. This is further confirmed by EDS spectra captured after the spot analysis on bright and grey areas of the back scattered images (Fig. 4c, d). As the spectra imply, the bright area is the iron rich area belongs to the aggregated α-Fe_2O_3 particles and the grey area corresponds to HA with out intense Fe peaks. The EDS spectrum (Fig. 4d) further substantiates the independent existence of HA and iron oxide grains in the sintered composite sample.

3.4 Biomineralisation—in vitro

The SEM images and the EDS analysis (Fig. 5) taken after the immersion in SBF indicate the status of relative biomineralisation occurred at HA with low temperature and high temperature phases of iron oxide. Figure 5a, b and c are SEM images and its EDS pattern of as prepared HA40Fe, sintered HA20Fe and HA40Fe, respectively. The sintered pellets in SBF result in the deposition of uniform globular aggregates of calcium phosphate over the pellet surfaces. The absence of Fe peaks in the EDS spectra of sintered pellets having hematite phase of iron oxide indicates the formation of thick apatite layer over the entire surface. The Fe peak visibility in the spectra of as prepared sample having magnetite phase of iron oxide is due to thin layer.kcb growth of calcium phosphate.

3.5 Cytotoxicity

The relative HOS metabolic activity among pure HA, as prepared HA40Fe (HA + Fe_3O_4), sintered HA20Fe (HA + 20% Fe_2O_3) and HA40Fe (HA + 40% Fe_2O_3) are graphically represented in Fig. 6. Among the two phases of iron oxide, MTT assay shows a high metabolic activity in hematite phase compared to the low temperature magnetite phase. A significant decrease in cell activity of the low temperature iron oxide phase compared with pure HA shows the decreased bioactivity of magnetite phase. Though the composite with 20% hematite shows an equal cell activity with pure HA, the statistically significant increase in cell viability between pure HA and composite with 40% hematite offers the possibility of utilizing the sample in tissue engineering applications.

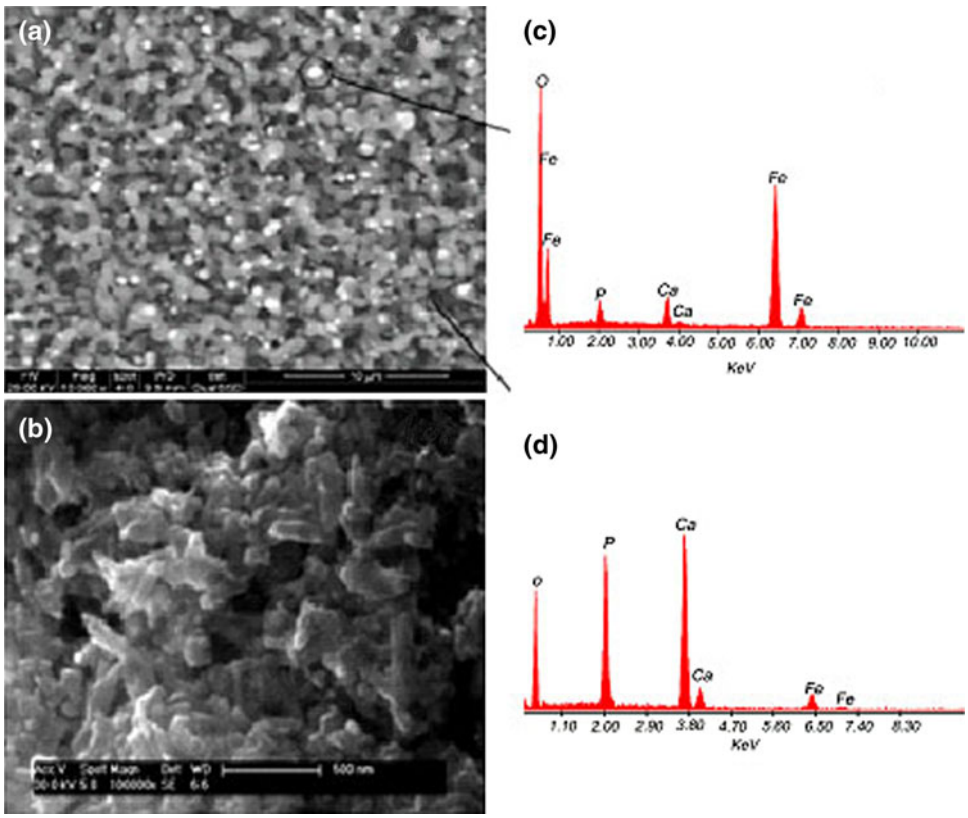

Fig. 4 SEM images of **b** as prepared composite **a** back scattered image of the sintered sample with the EDS spectrum of white **c** and the gray **d** region

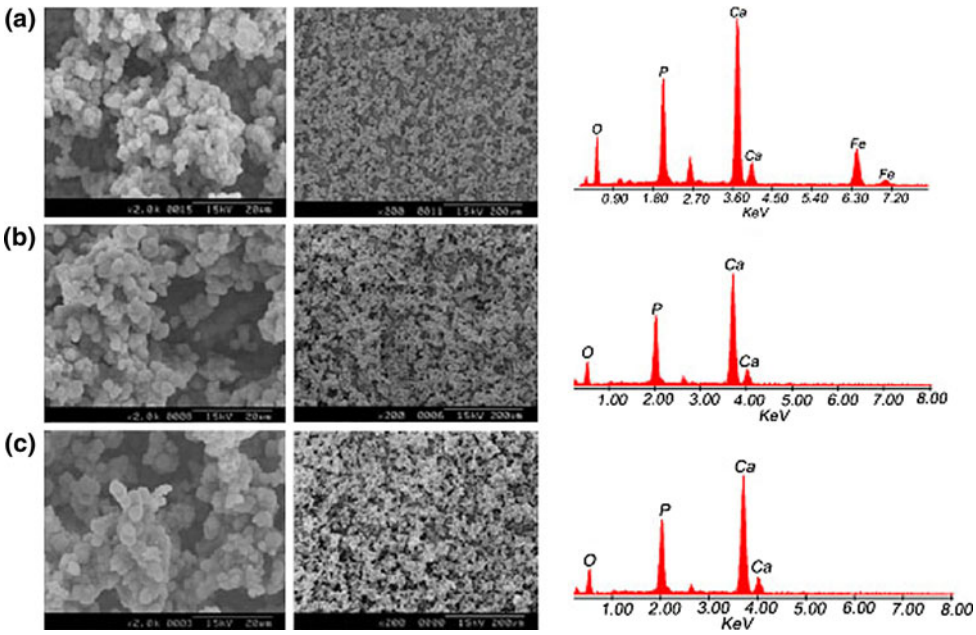

Fig. 5 SEM images and EDS spectra of pellets having **a** HA + magnetite, **b** HA + 20% hematite, **c** HA + 40% hematite taken after four days immersion in SBF

3.6 Cell adhesion

The in vitro cell culture studies demonstrated good adhesion of cells on the surface of the material. The SEM images taken on the 3rd day and 7th day are shown in Fig. 8. The micrographs of HA20Fe and HA40Fe cell seeded surfaces on the 3rd day (Fig. 7a, b) indicated a proliferating cell population which closely adhered to the surface of the material. But within 7 days, cells attached, adhered and spread out (cell phenomenology) in varying

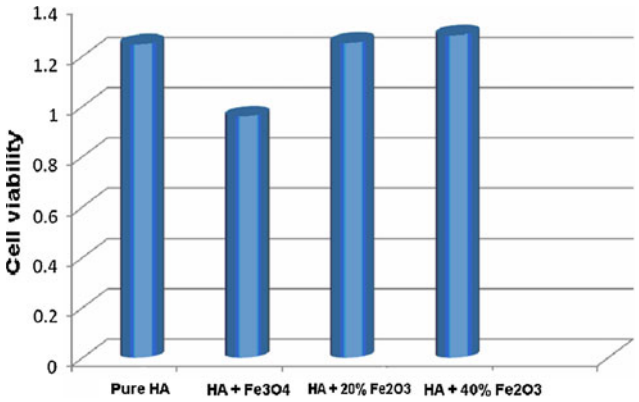

Fig. 6 Comparison of HOS cell viability of the prepared composite with pure HA and HA with magnetite phase of iron oxide

degrees on the surface of both HA20Fe and HA40Fe composites as evident from SEM micrographs (Fig. 7c, d). SEM evaluation over a period of time has demonstrated the initial adhesion of the cells, which at a later time point evolved into a cell sheet-like canopy over the material. The material thus provided a suitable substrate for the adhesion and proliferation of adipose tissue-derived stromal cells.

3.7 X-ray attenuation

A ranking of image contrast produced by HA with different percentage of iron oxide is shown in the Fig. 8. The image gray scale measurement gives 12% contrast for pure HA where as the 20, 40 and 60% samples exhibit 20, 35 and 50% contrast. The 100% contrast is assigned to immediate adjacent background. The HA contrast increases considerably with the increase of hematite phase. The linear variation in contrast enhancement with percentage of composition of the contrast media is graphically represented in Fig. 9.

If there is any variation in relative contrast due to the thickness of the sample during the X-ray attenuation in C-arm X-ray radiographic imaging system, Micro CT imaging would give a more accurate determination of the relative contrast by analyzing the slices of equal thickness of all the samples at a time.The 20 μm slices of the porous blocks obtained from micro CT analysis is as shown in Fig. 10. Though there is no marked difference in the attenuation between pure HA and HA20Fe; the significant increase in X-ray opacity shown by HA40Fe is clear from the CT image which gives a further conformation for the result from C-arm X-ray Imaging system.

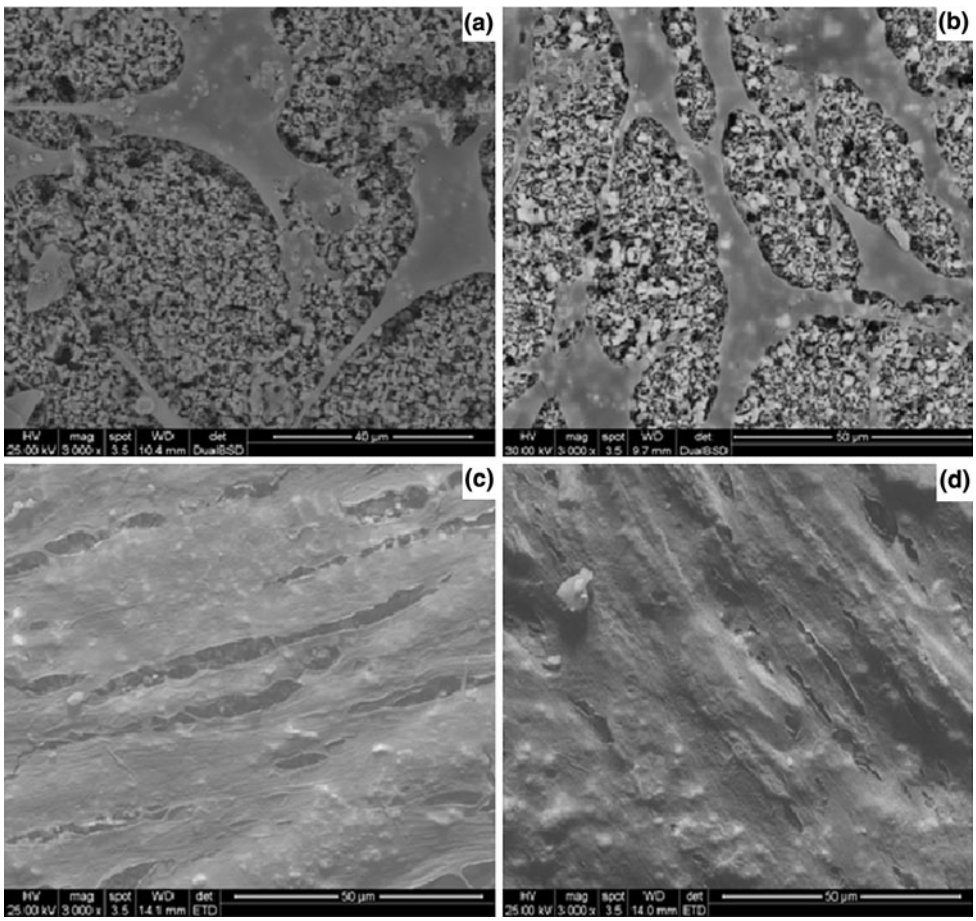

Fig. 7 The SEM micrograph of the cell seeded surface of
a HA20Fe after 3 days,
b HA40Fe after 3 days,
c HA20Fe after 7 days and
d HA40Fe after 7 days

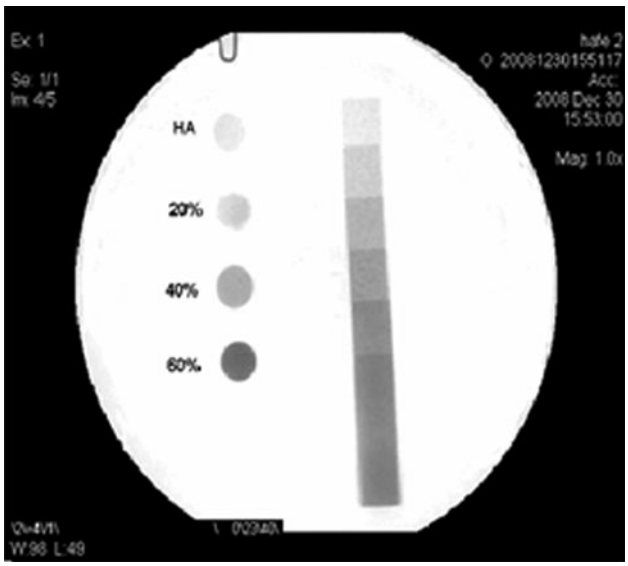

Fig. 8 X-ray images of pure HA, HA with 20, 40 and 60% hematite. An aluminum wedge is also included as the standard

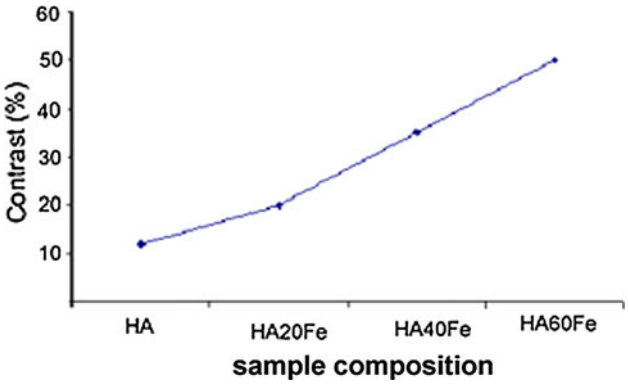

Fig. 9 Variation of measured contrast in X-ray images (digital) with respect to the percentage of composition of iron oxide

4 Discussion

The present synthesis methodology offers the preparation of nano iron oxide-HA composites with distinct HA and iron oxide phases. The precipitation of HA and nano iron oxide are pH sensitive and the crystallization of both takes place only at a high pH. The basic pH created in the system simultaneously brought about the precipitation of nano iron oxide particles together with HA crystallites. This simultaneous co-precipitation mechanism prevents the large order agglomeration of iron oxide nano particles. The XRD pattern revealed that during the process of sintering, phase identity of iron oxide and HA is unaltered and the absence of any other intermediate phase in the composite favors the mechanical and biological properties of HA. In an earlier

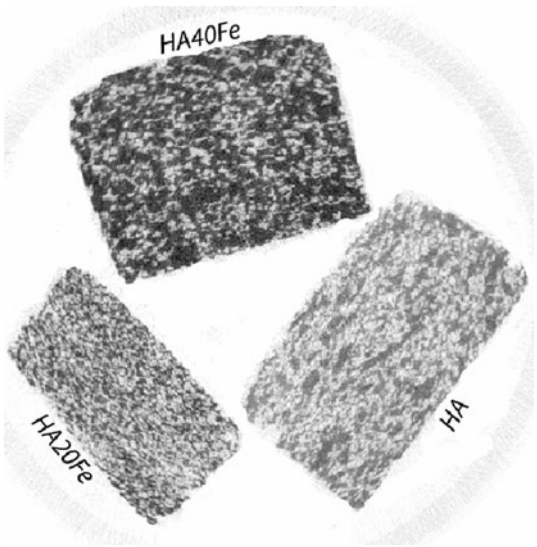

Fig. 10 μCT image of the porous samples which confirm the increased opacity shown by porous HA40Fe

study, various intermediated phases were formed during the sintering of iron oxide–HA composite prepared through ceramic route [17, 18]. The iron oxide nano particles attenuate X-rays and act as an opacifying agent without disturbing the phase purity, grain size as well as shape of HA in sintered state. The linear increment in X-ray attenuation with percentage of composition of iron oxide unfolds the radio-opacifying nature shown by hematite phase of iron oxide.

The in vitro biomineralisation studies and MTT assay results point out the better bioactivity of high temperature hematite phase rather than the low temperature magnetite phase of iron oxide. Cytotoxicity study also unveil that up to 40% iron oxide (hematite) is not detrimental to the osteoblast cell activity of HA. But the marginal increase in the cell activity of 40% iron oxide sample compared to pure HA is a surprising observation. Non-cytotoxic nature and good cell activity of the composite makes it a good candidate biomaterial for bone tissue engineering applications. A successful orthopedic implant requires a surface which is not only non-toxic but also allows the phenomenological behavior of bone cells [19]. The filamental extension of the cell seen in SEM images of both the samples support the fact that the contrast agent in HA matrix does not affect the cell adhesion nature and is independent of the percentage composition of iron oxide. Filamentous extensions of the cells was observed from the third day itself and a knitted cell sheet was observed after 7 days forming a canopy over the material. Cells that adhered and proliferated is expected to organise the ECM to convey signals (mechanical and chemical) influencing shape, actin cytoskeleton organization and transcription activity and subsequently to engineer a functional tissue.

5 Conclusion

X-ray contrast enhanced hydroxyapatite with good phase purity and increased osteoblast proliferation activity, has been synthesized through a co-precipitation route. The sintered nano-iron oxide HA composite show good bioactivity. The ability of the sintered composite material to support mature osteoblast cell lines and also adipose tissue-derived stromal have the potential for further therapeutic uses. This non-cytotoxic and cell proliferation activity can also be tried in future with various stem cells, for making it as a potential candidate for skeletal tissue engineering applications.

References

1. Lobenhoer P, Gerich T, Witte F, Tscherne H. Use of an injectable calcium phosphate bone cement in the treatment of tibial plateau fractures: a prospective study of twenty-six cases with twenty-month mean follow-up. J Orthop Trauma. 2002;16:143–9.
2. Urban K. Use of bioactive glass ceramics in the treatment of tibial plateau fractures. Acta Chir Orthop Traumatol Cech. 2002;69:295–301.
3. Easwer HV, Rajeev A, Varma HK, Vijayan S, Bhattacharya R. Cosmetic and radiological outcome following the use of synthetic hydroxyapatite porous-dense bilayer burr-hole button. Acta Neurochir. 2007;149:481–6.
4. Deb S, Abdulghani S, Behiri JC. Radiopacity in bone cements using an organo-bismuth compound. Biomaterials. 2002;23:3387–93.
5. Wallingford VH, Harriet GD, Kruty M. X-ray contrast media. I. Iodinated acylaminobenzoic acid. J Am Chem Soc. 1952;74:4365–43680.
6. Kjellson F, Almen T, Tanner KE, McCarthy ID, Lidgren L. Bone cement X-ray contrast media: a clinically relevant method of measuring their efficacy. J Biomed Mater Res. 2003;70B:354–61.
7. Sabokbar A, Fujikawa Y, Murray DW, Athanasou NA. Radio-opaque agents in bone cement increase bone resorption. J Bone Joint Surg. 1997;79:129–34.
8. Wimhurst J, Brooks R, Rushton N. The effects of particulate bone cement at the bone–implant interface. J Bone Joint Surg. 2001;83:588–92.
9. Adams DO. The granulomatous inflammatory response: a review. Am J Pathol. 1976;84:164–91.
10. Lazarus MD, Cuckler JM, Schumacher HR, Ducheyne P, Baker DG. Comparison of the inflammatory response to particulate polymethylmethacrylate debris with and without barium sulfate. J Orthop Res. 1994;12:532–41.
11. Ajay KG, Naregalkar RR, Vikas DV, Mona G. Recent advances on surface engineering of magnetic iron oxide nanoparticles and their biomedical applications. Nanomedicine. 2007;2:23–39.
12. AnHui Lu, Salabas EL, Ferdi S. Nanoparticles: synthesis, protection, functionalisation and application. Angew Chem Int Ed. 2007;46:1222–44.
13. Maite L, Nadia C, Ching HT, Xiao WT, David C, Scadden DT, et al. Tat peptide-derivatized magnetic nanoparticles allow in vivo tracking and recovery of progenitor cells. Nat Biotechnol. 2000;18:410–4.
14. Seyda B, Deverraux AJ, Paul E, Laibinis T, Alan H. Protein separations using colloidal magnetic nanoparticles. Biotechnol Prog. 2003;19:477–84.
15. Kokubo T, Kim HM, Kawashita M. Novel bioactive materials with different mechanical properties. Biomaterials. 2003;24:2161–75.
16. Williamson GK, Hall WH. X-ray line broadening from filed aluminium and volfram. Acta Metall 1953;1:22–31.
17. Filho FP, Nogueira RE, Graca MPF, Valente MA, Sombra ASB, Silva CC. Structural and mechanical study of the sintering effect in hydroxyapatite doped with iron oxide. Physica B. 2008;403:3826–9.
18. Silva CC, Filho FP, Graca MFP, Valente MA, Sombra ASB. Dielectric and structural characterization of iron oxide added to hydroxyapatite. Bull Mater Sci. 2008;31:635.
19. Hunter A, Archer CW, Walker PS, Blunn GW. Attachment and proliferation of osteoblasts and fibroblasts on biomaterials for orthopedic use. Biomaterials. 1995;16:287–95.